2. Literature Review

2.1 General

Pillars are a block of coal left between excavations whose primary objective is to provide natural support. The barrier pillars are a type of pillar that provides isolation between the panels or the mines. The barrier pillars with a water reservoir at one end are known as protective water barrier pillars. The behaviour of a protective water barrier pillar is influenced by the pillar itself, apart from the roof and floor interface and the associated strata.

The evaluation of hydro-mechanical performances and an objective-oriented design of inter-mine barrier pillars have been a grey area for Indian geo-mining conditions. The mines have been operating with an unknown level of the potential risk of inundation on one side and causing loss of valuable resources on the other side. Hence, the literature review has been conducted to identify the knowledge gap in existing know-how and formulation of the objective for this research work. The various aspects of the pillar design have been reviewed in the literature to understand the underlying phenomenon and to formulate a basis for the design of PWBP.

This chapter is organised into seven sections: prevailing understanding of PWBP design, global experiences, the mechanical design of pillars, effect of interface on the pillar behaviour, constitutive behaviour of the pillar, mechanism of fluid flow through porous media, essential considerations in PWBP design, and regulatory & operational provisions w.r.t. the Indian coal mines.

2.2 Prevailing Understanding

The existing approach for the design of PWBP are summarised in Table 2.1.

Table 2.1. Existing design approaches (Kendorski and Bunnell 2007; DGMS 2017)

Sl. No.	Name	Pillar Width, m	Description
i	Dunn's Rule	$\frac{(D-54.86)}{20}+4.57$ …(2.1)	Suggests a barrier width of 4.57m at a cover depth of 54.86m; the width increases by 0.9 m for an increase in cover depth of 18.29m
ii	Ashley's Method or Pennsylvania Mine Inspector's Equation	$\frac{D}{10}+4h+6.1$ …(2.2)	D is the water head if it is greater than the cover depth, potential equation as considered the depth, seam thickness, and water head
iii	Ash and Eaton's Impoundment Equation	$\frac{D}{2.35}+15.24$ …(2.3)	It does not consider the strength and hydraulic properties.
iv	Outcrop Water Barrier Pillars	$\frac{D}{3.28}+15.24$ …(2.4)	Developed after several failures of undersized protective water barrier pillars against a large water head in Kentucky, USA, the effect of the strength not considered
v	Old English Barrier Pillar Law	$\frac{Hh}{30.48}+5h$ …(2.5)	not recommended for extraction height greater than 4.57m, strength not considered
vi	The Pressure Arch Method	$2.625 * \left(\frac{D}{20}+6.1\right)$ …(2.6)	suggested for a cover depth of 122-853m, does not consider the strength and hydraulic properties
vii	British Coal Rule of Thumb	$\frac{D}{10}+13.72$ …(2.7)	used in British mines, does not consider the strength and hydraulic properties

Where D is cover depth in m, h is extraction height in m, and H is water head in m

These empirical designs consider an adequate allowance for stress, permeability, additional hydraulic pressure, undermining, etc. (Singh et al., 1982). Using a higher FOS for these accounts leads to overdesigning the barrier pillar.

A closer evaluation of the overall design approach suggests that depth of working is a unanimously considered parameter for deciding the size of PWBP. A few of the methods have considered the extraction height along with the cover depth for this purpose. However, these approaches are oversimplified as they completely ignore the effect of strength and the hydraulic characteristics of the rock formation. For the cover depth of 100-350 m and extraction height of 3 m, the width of PWBP, as estimated by these approaches, varies between 7 to 164 m. A pillar width of 25-30 m at a cover depth of 100 m and a pillar width of 50m at a cover depth of 350m seems to be the most common estimate from these approaches. Although these approaches provide a preliminary design of PWBP, they cannot project their hydraulic performance for different water heads nor offer any scientific explanation for these proposed solutions.

The design of a protective pillar is complex owing to its permanent life expectancy and the requirement of hydro-mechanical consideration in the analysis. Under such conditions, both regional and local conditions govern their stability. The regional conditions determine the load acting on the pillar, depending on the depth, stiffness of the overlying strata, extraction ratio, and hydraulic pressure gradient. The local conditions determine the pillar strength, which depends on the pillar dimension, hydraulic conductivity, quality of the roof, pillar, floor, and the associated interfaces (Luo et al., 2001, Kesseru, 1978).

Pillar width is an imperative factor in defining the stability of protective barrier pillars. The confining stresses are strongly correlated with the change in the width of the water barrier. The seepage rate through the barrier and the ability to withstand high hydraulic heads call for wider protective pillars. The seepage rate decreases or remains under control as it delays the flow and indirectly contains the danger from piping failure and water inrush. An increase in

pillar width significantly impacts the seepage rate pattern as the pillar becomes both mechanically and hydraulically stable. The coal pillar subjected to the redistributed load of overlying strata tends to form four distinct zones: elastic, yielding, crushed, and slumped (Figures 2.1-2.2), also known as the core, intermediate, transition, and rib zones. Morsy (2003) marked the three distinct zones in the pillars as the core zone, intermediate zone, and rib zone (Figure 2.3). The pillars have a lower strength in the yield zone than in the elastic zone. The induced stress causes a large lateral strain in the pillar. Sometimes, the transformation of the core zone to the yield zone can be sudden, leading to the collapse of the complete pillar. Hence, the mechanical stability of the pillar largely depends on the extent of the yield zone.

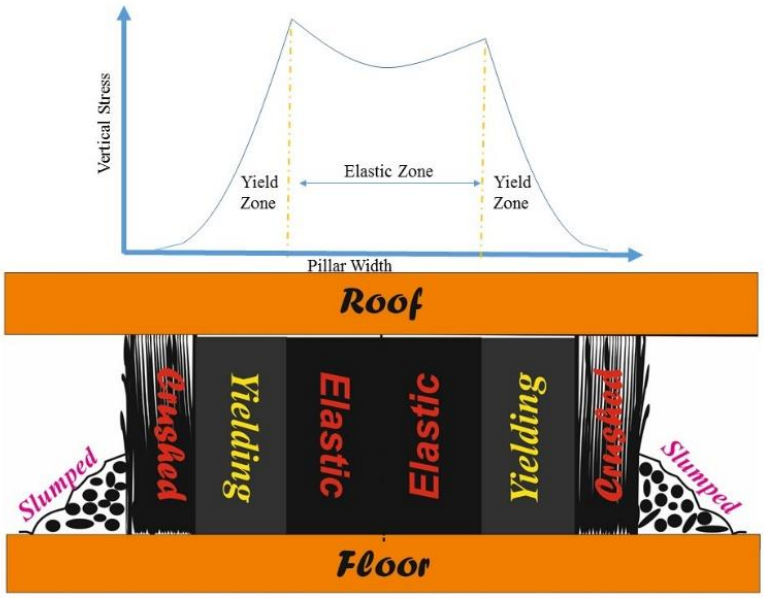

Figure 2.1. Sectional view showing vertical stress redistribution and distinct zones in a pillar

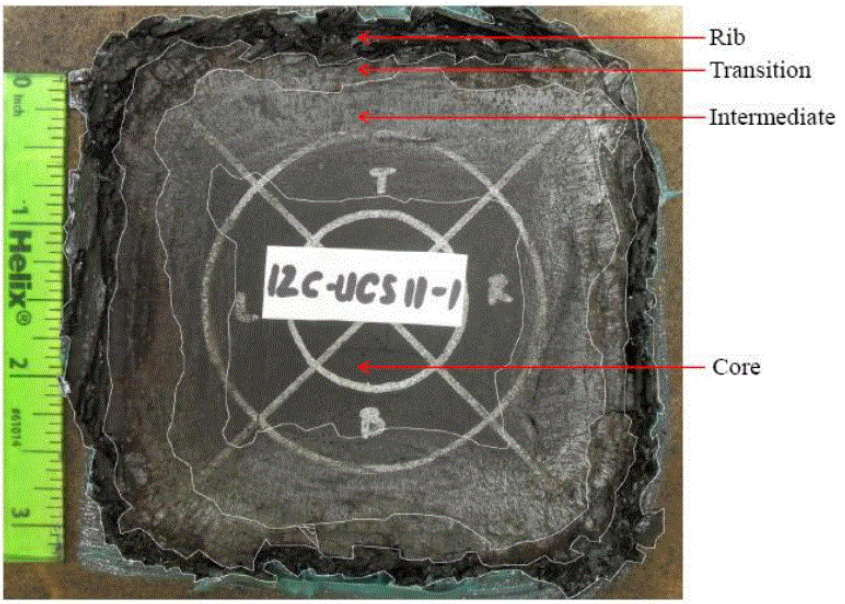

Figure 2.2. Plan view of the four distinct zones in a coal sample of w/h=12 (Prassetyo, 2011)

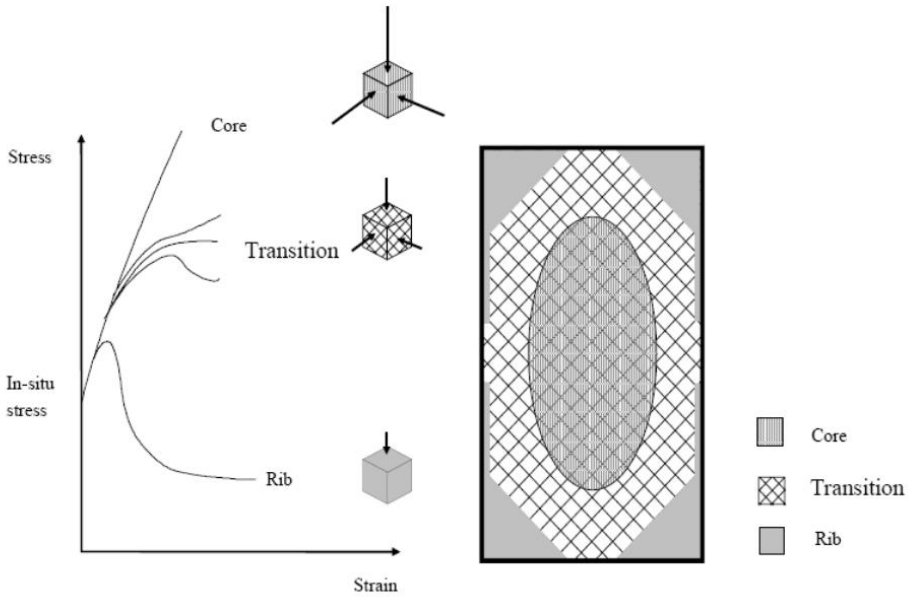

Figure 2.3. The three zones in the pillar (Morsy, 2003)

In general, protective water barrier pillars are squat in size (width/height >10). They have high strength owing to considerable confinement to their cores and frictional resistance at the roof-floor and pillar interfaces. A weak interface consisting of a soft clay band can facilitate increased dilation of pillars, followed by higher lateral strain and reduced core confinement, resulting in the overall weakening of the pillar (Lonnies, 2017). The stresses near the edge of the pillar are the highest before it begins to yield. When the induced stress exceeds the strength, the pillar begins to yield. As a result, the edges shed the load, transferring it farther inside until the confined core accepts the redistributed load. The pillars continue to weaken due to the yielding and load transfer, ultimately causing the failure of the pillar. Cook et al. (1971) and Wagner (1974) concluded that the core carries the maximum load after the failure of the pillar (Figure 2.4).

The rate of failure or load shedding is strongly determined by the width-to-height ratio. As the width/height ratio increases, the unloading rate decreases, and the post-failure behaviour of the structure changes from strain-softening to plastic yield and strain-hardening (Figure 2.5). A pillar with a high w/h ratio acts as an abutment, and no significant load shedding occurs in such a case.

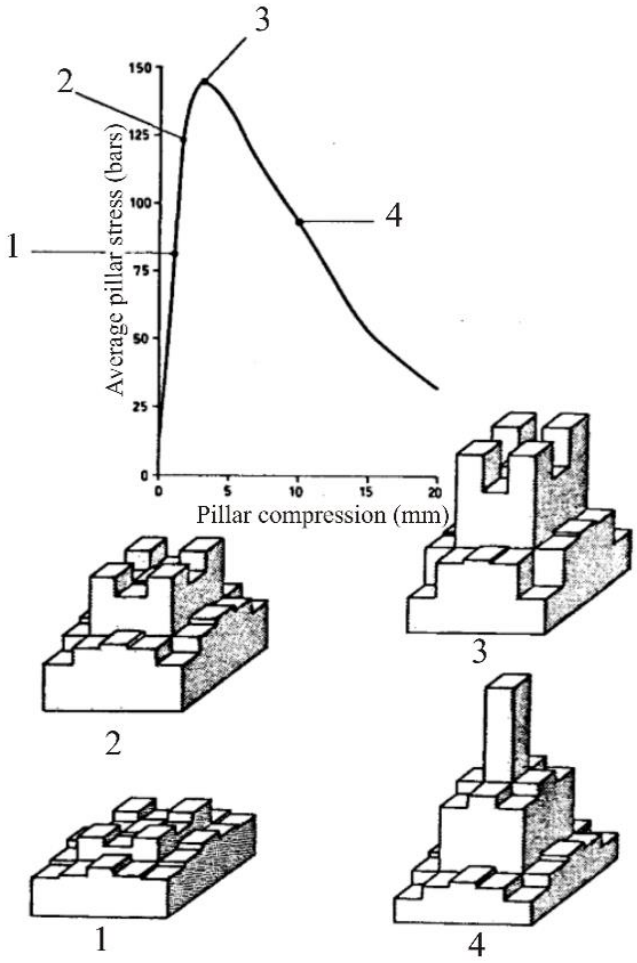

Figure 2.4. Stress-strain characteristics and failure behaviour of an in-situ pillar of 2 m width and 1 m height at different stages of loading (Wagner, 1974)

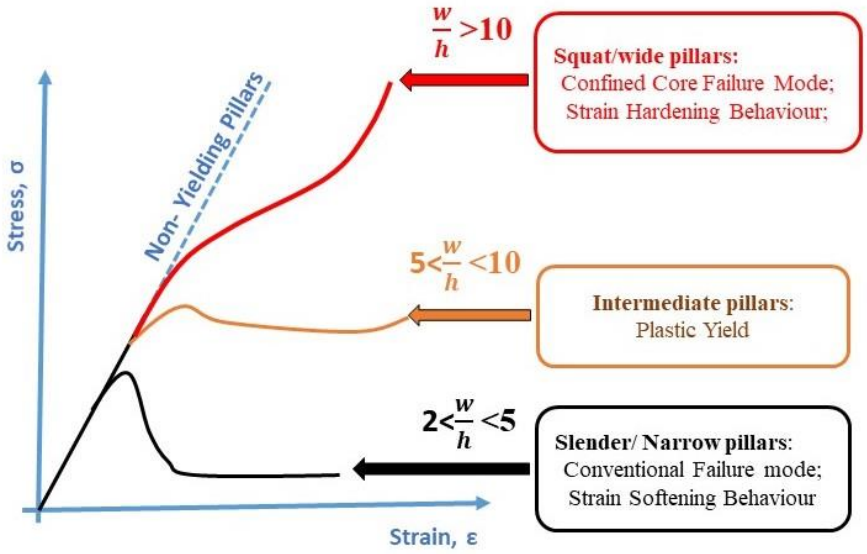

Figure 2.5. Effect of w/h ratio on the constitutive behaviour and failure mode of Pillar

Long-term immersion of coal in water leads to its saturation, reducing its mechanical strength. Rock expansion due to the intrusion of water also causes a reduction in the modulus of elasticity and rock strength (Liu, 2010). Parameters like cohesion, internal friction angle, uniaxial compressive strength, and tensile strength of coal decrease as it comes in contact with water (Guo, 2010; Das, 2016). The elastic modulus of coal reduces up to 8% and remains stable (Wang et al. 2019). When the moisture content is greater than 15%, the compressive strength of the coal drops to 5% of its strength under dry conditions. The increasing stress condition further intensifies the deterioration of the stability condition as water saturation penetrates deep inside the barrier pillar, aggravating the situation and leading to interconnections across the barrier.

In addition to mechanical failure, piping failure resulting from excessive water seepage rate is also possible. A piping failure of a barrier pillar refers to the process where water moves

through the rock mass, forming the pillar in a coal mine and eroding the minerals and joint-filling materials, creating voids or channels that weaken the support provided by the pillar. This can lead to the collapse of the pillar and potentially cause inundation in the mine.

The behaviour of the pillar and the roof is also governed by their relative stiffness (Mark, 1987). When the post-failure stiffness of the roof strata is greater than the post-peak stiffness of the pillar, the pillar unloads in a controlled manner. However, the stiffness of the roof reduces with an increase in the excavation span. Hence, the pillar undergoes an uncontrolled or sudden collapse when the loading system's post-failure stiffness gets lower than the pillar.

A protective water barrier pillar may be considered to have failed if the seepage rate is high enough to cause piping failure or cannot contain the water in the reservoir. The factors defining failure are peak strength, critical strain, and the rate of seepage (Kesseru, 1982; Kendorski & Bunnell, 2007; Luo et al., 2001). The rate of unloading after passing the peak strength determines the post-failure mechanical performance of the pillar, while the rate of seepage determines its hydraulic performance. In this regard, the change in hydraulic resistance of the pillar with a change in hydraulic pressure and mining conditions is of paramount interest. Although the mechanical and hydraulic performances are strongly correlated, they need to be investigated in detail for the rational design of such pillars.

2.3 Global Experience

The global mining community has suffered a considerable loss in terms of the lives of miners, machinery, mineral resources, and capital due to inundation disasters in the mines. Table 2.2 compiles the inundation cases worldwide. The primary reason for such inundation is the faulty design of PWBP. In some cases, the PWBP of otherwise sufficient size failed to perform its design function due to the presence of a fault plane in the close vicinity. A careful

study of these cases indicates that the inadequate size of the barrier has been a significant cause of inundation disasters in active mine working. The failure of PWBP has also been triggered by blasting and mine explosions in a few cases.

Table 2.2. Significant mine disaster due to inundation (Bloemendaal, 2014; Dash et al., 2016; DGMS, 2005, 2006, 2017; ICM, 1891, 1892, 1898; MIR, 2020; NMRS, 2020; Ramlu, 1991; Vutukuri and Singh, 1995; Whitworth, 2013)

Sl. No.	Name of the Mine	Date of Occurrence	No. of lives lost	Observations
(i)	Loyabad Colliery, India	16.01.1935	11	A development gallery punctured into abandoned workings of the same mine.
(ii)	Newton Chikli Colliery, India	10.12.1954	63	Mine was inundated due to an inrush of water from the abandoned working of the top seam.
(iii)	Burra Dhemo Colliery, India	26.09.1956	28	An accumulation of surface water entered the underground workings through pot-hole subsidence.
(iv)	Central Bhowrah Colliery, India	20.02.1958	23	Mine was inundated due to an inrush of water from the abandoned workings of Sonardih Colliery.
(v)	Silewara Colliery, India	18.11.1975	10	Flooding of the mine was caused by the failure of a thin barrier pillar separating the development working from the waterlogged working.
(vi)	Chasnalla Colliery, India	27.12.1975	375	In Degree-III gassy mine, a spark generated from equipment whose flameproof enclosure went wrong and ignited a pocket of firedamp. The firedamp explosion raised the coal dust cloud and ignition, which led to a coal dust explosion. This explosion punctured the inter-mine barrier to a water reservoir.
(vii)	Central Saunda Colliery, India	16.09.1976	10	Water from the flooded Nakari river entered the underground workings of the Hathidari seam through cracks in the subsided goaf area.
(viii)	Hurriladih Colliery, India	14.09.1983	19	A large quantity of water came down from the top section of the seam and flooded the dip side workings, drowning all the workers employed there.

(ix)	Mahabir Colliery, India	13.11.1989	6	Flooding was caused by an inrush of water from the overlying Ningah seam to the Narainkuri seam
(x)	Rajpura Dariba Mine, India	28.08.1994	13	The cement plug at the draw level of stope T-17 gave away, and about 8000 m^3 of the slurry, with the broken pieces of the plug, fell to the lower levels and flowed to the main shaft.
(xi)	Bagdigi Colliery, India	02.02.2001	29	The incompetent pillar of 20-27 m width (some reports suggest it was only 10m at failure) separating Bagdigi mine from the water-logged and abandoned Jairampur mine at 240m depth. A routine blasting destroyed the underground barrier between Bagdiggi and Jairampur collieries. The reduced thickness of the barrier pillar resulted in its failure under water pressure from the adjacent flooded mine.
(xii)	GDK-7 Project, India	16.06.2003	17	The incompetent size of the barrier pillar near the stowed section was filled with water filled in spaces of stowing material.
(xiii)	Central Saunda Colliery, India	15.06.2005	14	The incompetent size of the barrier led to a connection between the Bansgarha seam and the overlying water-logged abandoned workings of the Hathidari seam.
(xiv)	North Virginia Mine, USA	Not Available (NA)	NA	Ineffective barrier pillar between the active mine and abandoned waterlogged working. The barrier also had geological structural anomalies, contributing significantly to its failure.
(xv)	Gretley Coal Mine, Australia	11.1996	4	The drill machine broke into the abandoned waterlogged working.
(xvi)	Audley Colliery, UK	14.01.1895	77	An incompetent water barrier pillar accidentally broke into the abandoned working
(xvii)	White Ash Mine, USA	09.09.1889	10	Mine fire weakened the incompetent mine barrier leading to a connection with the abandoned waterlogged working.

(xviii)	Spring Mountain Mine, USA	04.02.1891	9	Incompetent size of the barrier
(xix)	Lytle Mine, USA	20.04.1892	10	Incompetent size of barrier and incorrect surveying.
(xx)	Kaska William Colliery, USA	09.05.1898	6	The accidental connection of the under-construction shaft with the waterlogged tunnel
(xxi)	Redding Colliery, UK	25.09.1923	40	Water filled into the shaft after the failure of the barrier.
(xxii)	Montagu Colliery, UK	30.03.1925	38	Incompetent size of the barrier
(xxiii)	The North Virginia Mine, USA	NA		A barrier pillar of 143m wide was inadequate to prevent the influx of water from an abandoned working.

According to Hungarian mine safety legislation, a critical hydraulic gradient determines the size of protective water barrier pillars and predicts the severity of water seepage rate (Kesseru, 1978; Hungarian mine safety authority, 1975). Data from 1,000 mines suggested a maximum water inflow of 2.5 m^3/min if the hydraulic gradient is less than 5 m/m (Kesseru, 1970). These observations align with Terzaghi (1931) and Lampl (1959). The piping failure may start when the prevailing hydraulic gradient exceeds the critical limit. Kesseru (1969,1976, 1978) opined that critical hydraulic gradient strongly depends on rock stress conditions and material properties. Numerical modelling is the best tool for its determination (Harr et al., 1978).

McCoy et al. (2006) presented Darcy's law-based approach (Equation 2.8) to estimate leakage across barriers through "n" segments of variable sizes.

$$Q_{pump} = \sum_{i=1}^{n} K_h b L_i \frac{\Delta h_i}{w_i} \quad \ldots(2.8)$$

Where, Q_{pump} = pumping discharge, m^3/s

K_h = horizontal hydraulic conductivity, m/s

b = mine-aquifer thickness or height of seepage face under confined conditions, m

L_i = barrier segment length, m

Δh_i = head difference across a barrier, m, and

w_i = barrier width, m.

Miller and Thompson (1974) suggested Equation (2.9) for estimating seepage rate through the barrier pillar.

$$Q = \frac{0.5D\frac{Kw}{h}}{\frac{w}{0.5h}} = 0.25\frac{DK_w}{w} \quad \ldots(2.9)$$

Where, Q = flow rate, m^3/s

D = cover depth, m

K = permeability coefficient, m/s

w = pillar width, m, and

h = height of the pillar, m.

The key factors influencing the performance of protective water barrier pillars are roof-pillar-floor interfaces, the behaviour of surrounding strata, rock mass strength, permeability, porosity, water head, and water viscosity (Esterhuizen, 1997). Kesseru (1982) opined that the design of PWBP should mainly consider the seepage rate. Determining the hydraulic gradient and the yield zone in the pillar are also important. The minimum size of the pillar should correspond to the critical hydraulic gradient.

Kendorski and Bunnell (2007) conducted a coupled numerical simulation using a two-dimensional Finite difference model to estimate induced strain and flow characteristics in the PWBP. He concluded that the rock behaved elastically without any significant change in the flow pathway below the threshold strain of 0.1%. Accordingly, the coal pillar of 107 m width at a cover depth of 580 m was evaluated to have a low geotechnical but moderate hydrological risk. Chen et al. (2017) considered coupled simulation to analyse hydraulic pressure and seepage rate and suggested a 30.7 m wide pillar at 509 m depth.

McCoy et al. (1992) studied the leakage rate across coal mine barriers of 15 to 50 m width, considering the horizontal hydraulic conductivity of the coal seam, the thickness of the barrier, water head, and the orientation of the barrier w.r.t. the cleavage planes in the coal wall. Hydro-mechanical coupling allows the simulation of the disturbance induced by the excavation in terms of porosity, stress distribution, pore pressure, and fluid flow (Chen, 2017). Seepage rate, inrush, and failure can also be considered using a combination of mechanical and hydraulic simulations (Wang, 2019). Luo et al. (2001) focused on the impact of ground stress on rock permeability and water seepage rate to assess stress distribution and flow across the barrier pillar. The study revealed that seepage through the pillar was parallel to bedding planes, and it was higher through the pillar as compared to the roof and floor. They also observed an increase in seepage with the increase in the yield zones. The seepage rate increased with the yield zones, which could result in pillar instability.

2.4 Mechanical Stability of Pillar

The stability of PWBP is governed by its mechanical and hydraulic performance. Hence, it is imperative to study the parameters influencing the mechanical stability of pillars.

An extensive attempt has been made to understand the behaviour of coal pillars by laboratory testing of rock samples (Wang et al., 2017; Medhurst and Brown, 1998; Zhou, 2018), in-situ testing, numerical modelling, and back analysis of pillar behaviour (Bieniawski and Van, 1975; Madden, 1990). Although these efforts were limited regarding the loading system and interface conditions, they still provided valuable insight into the behavioural differences in material and structure, the post-failure behaviour, the strength of the core, the circumferential portions of a pillar, etc.

Bunting (1911) carried out laboratory experiments and back analysis for failed pillar cases and concluded that the pillar strength was a function of the width and height of the pillars. Before the formulation of the Salamon and Munro (1967) equation, several empirical relations were suggested by Zern (1928), Greenwald et al. (1941), Gaddy (1956), and Holland and Gaddy (1964) as a function of specimen strength, width, and height of the pillars. Salamon and Munro (1967) used the back analysis technique to develop an empirical equation for pillar strength determination. They analysed the performance of the 27 failed and 97 stable pillars, with a w/h ratio varying from 0.9 to 8.8. The load on the pillar estimated by tributary area theory measures the load as a function of the in-situ stresses acting on the pillar and the extent of extraction around it. Sheorey (1986) modified the Salamon and Munro (1967) pillar strength equation for Indian geo-mining conditions.

Hoek (1966) explored the feasibility of in-situ testing for a sample of up to 2 m in height and width and w/h ratio of 0.5 - 3.4. Cook et al. (1971) and Wagner (1974, 1980) viewed that the pillars withstand the load of the overlying strata even after their failure. The failure starts at the circumference and advances towards the core. Wagner (1980) suggested using ‘effective width’ instead of ‘width’ for rectangular pillars to estimate pillar strength

Until 1970, the research for pillar design was primarily concentrated on the slender pillar as most mining activities were at shallow cover depths. Subsequently, the cover depth has increased, and the research focus has also been oriented towards squat and long-sized pillars. Logie and Matheson (1982) updated the Bieniawski and Van (1975) formula to accommodate the effect of higher cover depth. Mark and Chase (1997) opined that the pillar strength of rectangular squat pillars is a function of the width-to-height and width-to-length ratio of the pillar. Wilson (1983) advanced the pillar strength equation for rectangular and long pillars. Sheorey (1992) developed Equation (2.10) to estimate pillar strength for Indian coal mines.

$$S_p = 0.27\sigma_c h^{-0.36} + \left(\frac{D}{250} + 1\right)\left(\frac{w}{h} - 1\right) \quad \ldots(2.10)$$

Where, s_p = pillar strength, MPa,

σ_c = strength of the 25 mm cubical coal specimen, MPa,

w = pillar width, m,

h = pillar height, m, and

D = cover depth, m.

Sinha and Walton (2019b) conducted a numerical modelling study to study the influence of the width and length on the pillar strength. They found that the width-to-height ratio is susceptible to strength, whereas the length-to-width ratio has no significant impact.

Several in-situ testing, laboratory testing, and numerical modelling efforts have been made to characterise the stress-strain behaviour of rocks (Wawersik, 1968; Das, 1986; Zhao and Cai, 2010; Medhurst and Brown, 1998). Wawersik (1968) classified rock post-failure

behaviour into two classes based on the axial loading of a cylindrical specimen. Class I represents ductile behaviour, while class II represents brittle nature. Earlier, it was challenging to capture the constitutive behaviour, especially for small w/h ratio specimens, but stiff servo-controlled machines such as the Material Testing System (MTS 2022) have made it convenient for researchers.

Das (1986) conducted laboratory testing to develop constitutive behaviour for six Indian coal seams. The NX-size coal specimens were tested for a w/h ratio of 0.5 to 13.5. The results of the laboratory studies indicated brittle-type post-failure behaviour of pillars for a w/h ratio of 0.5–3, strain-softening behaviour for a w/h ratio of 4.5–9, and strain-hardening behaviour for a w/h ratio of 13.5. With an increase in the w/h ratio, the post-failure slope changed from negative to positive, implying that the post-failure strength increases with the w/h ratio (Figure 2.6).

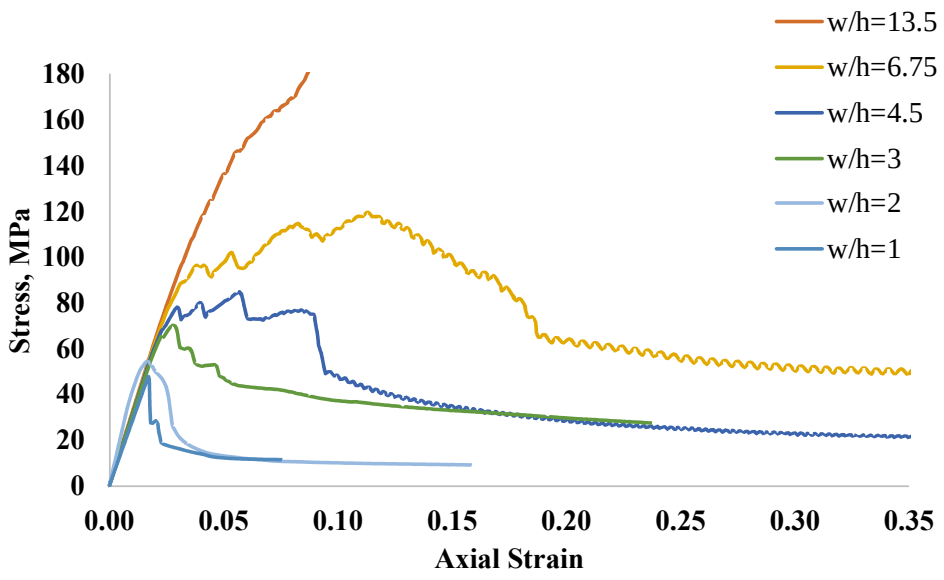

Figure 2.6. Laboratory observed stress-strain behaviour of Kenda Seam specimens

2.5 Strain Softening Behaviour of Pillars

Several numerical modelling-based studies have been carried out to match the laboratory-observed peak strength and post-peak behaviour of coal pillars for varying width-to-height ratios. Mohan et al. (2001) modelled the strain softening parameter by increasing the cohesion by 10% and reducing the friction angle by 5° at zero shear strain. The residual values of cohesion and friction angle were decreased by 10 % at 1 % of plastic shear strain, maintaining a constant drop rate. Esterhuizen and Barczak (2006) proposed a 90 % decrease in cohesion over 0.5 % plastic strain. Zhang et al. (2018) used a 90 % reduction in cohesion and a 6° reduction in friction over 5 % plastic strain.

The dilation angle is an intrinsic property of rock that measures its dilation behaviour. Several studies (Detournay, 1986; Medhurst, 1996; Alejano and Alonso, 2005; Zhao and Cai, 2010; Walton and Diederichs, 2015) have been made to incorporate the effect of dilation on the strain-softening behaviour of the pillars. Detorney (1986) developed an exponential function for dilation mobilisation and revealed that dilation should be the function of confining stress and plastic strain. Medhurst (1996) showed that the dilation angle decreases with increased confining pressure. Alejano and Alonso (2005) further analysed the findings of Medhurst (1996) and developed a plastic strain-controlled dilation decay model (Equation 2.11-2.15).

$$(\sigma_3, \gamma^p) = \begin{cases} \dfrac{\alpha \gamma^p \varphi_{peak}}{e^{\left(\frac{\alpha-1}{\alpha}\right)}\gamma_m} & when \quad \gamma^p < e^{\left(\frac{\alpha-1}{\alpha}\right)}\gamma_m \\ \varphi_{peak}\left(\alpha ln\left(\dfrac{\gamma^p}{\gamma_m}\right)+1\right) & when\ e^{\left(\frac{\alpha-1}{\alpha}\right)}\gamma_m \le \gamma^p < \gamma_m \\ \varphi_{peak}\, e^{\left(\frac{-(\gamma^p-\gamma_m)}{\gamma^*}\right)} & when \quad \gamma^p \ge \gamma_m \end{cases} \qquad \ldots(2.11)$$

$$\alpha = \alpha_0 + \alpha' \sigma_3 \qquad \ldots(2.12)$$

$$\gamma^* = \begin{cases} \gamma_0 & when\ \sigma_3 = 0 \\ \gamma^* & when\ \sigma_3 \neq 0 \end{cases} \quad \ldots(2.13)$$

$$\varphi_{peak}(\sigma_3) = \frac{\phi_{peak}}{1+log_{10}\left(\frac{UCS}{\sigma_3+0.1}\right)} \quad \ldots(2.14)$$

$$\gamma^p = \in_1^p - \in_3^p \quad \ldots(2.15)$$

Where, α_0 determines the curvature of the pre-mobilization for zero confinement,

α' determines the pre-mobilization curvature changes as a function of σ_3,

ϕ_{peak} = peak friction angle of coal, °,

UCS = uniaxial compressive strength of coal, MPa,

σ_3 = horizontal stress, MPa,

γ_m = plastic shear strain at peak dilation,

γ_0 = decay rate of the dilation angle post-mobilization for zero confinement,

γ^* = decay rate of the dilation angle post-mobilisation for non-zero confinement,

$\in_1^p$ = major principal plastic strain increment, and

$\in_3^p$ = minor principal plastic strain increment.

Zhao and Cai (2010) also developed a plastic strain-based dilation decay and mobilisation model. Walton and Diederichs (2015) opined that while Alejano and Alonso's model is limited to sedimentary rocks, the implementation of Zhao and Cai's model is complicated.

2.6 Effect of Interface on Pillar Behaviour

Studies conducted by various researchers (Peng, 1978; Wagner, 1980; Babcock, 1985; Iannacchione, 1990; Gale, 1999; Lu et al., 2008; Esterhuizen, 2010; Prassetyo, 2011; Rashed and Peng, 2015) have revealed the importance of Roof-Pillar-Floor interfaces on pillar behaviour. The properties of the interface are imperative for an accurate estimate of the strength and post-failure behaviour of the pillars. The laboratory testing conducted by Peng (1978), Wagner (1980), Prassetyo (2011), and Rashed and Peng (2015) revealed that variation in interface shear strength influences the strength of the cylindrical specimens. Peng (1978) observed that this variation could be up to 100 % depending on the shear strength of the interface. Wagner (1980), Prassetyo (2011), and Rashed and Peng (2015) also observed a change in the mode of failure with the variation in the shear strength properties of the interface.

Iannacchione (1990) reported that numerical models produce unrealistically high horizontal stresses in the pillar without the interface in the model. This effect was more pronounced in the squat pillars (w/h > 10). He suggested that the cohesion and friction angle range be 0–1.03 MPa and 10–20° for modelling clay-filled interfaces. Lu et al. (2008) also observed an increase in the minimum principal stress with an increase in the shear strength of the interface. Esterhuizen et al. (2010) incorporated the interface cohesion of 0.1 MPa, friction angle of 25°, zero tensile strength, normal stiffness of 100 GPa/m, and shear stiffness of 50 GPa/m for simulating the field observed stress gradient at the pillar edges. Prassetyo (2011) conducted a direct shear test on three different interface types to establish their internal friction angle and categorised the friction values of 22° as ‘high’, 12° as ‘medium’, and 7° as ‘low’.

Lonnies (2017) optioned that most interface infill material is a thin layer of clay that water can easily wash away. Using Iannacchione's (1990) range for cohesion and friction angle, he classified the interface strength as ‘high’, ‘medium’, and ‘low’ for friction angle and cohesion values of 25° and 1.38 MPa, 17° and 0.7 MPa, and 10° and 0 MPa, respectively.

2.7 Mechanism of Fluid Flow through Porous Media

The studies related to geo-fluid interaction started in the soil mechanics domain. Terzaghi (1921) proposed the effective stress theory for soil-fluid interaction wherein the pressure developed in the saturated soil was obtained as the sum of the effective pressure on the matrix and the pore pressure. The same was later extended to understand rock-fluid interaction. The seepage outflow through the PWBP can be simulated using Darcy's law (Equation 2.16), which states the relationship between the discharge rate, hydrostatic gradient, and permeability coefficient.

$$q = -k\frac{\partial p}{\partial x} \qquad \ldots(2.16)$$

Where q = specific discharge vector,

k = mobility coefficient (Equation 2.17),

p = fluid pressure, and

x = flow length.

$$\text{Mobility coefficient, k} = \frac{\text{Intrinsic permeability}}{\text{Fluid dynamic viscosity}} \qquad \ldots(2.17)$$

The porosity and permeability of the coal seam and the associated rocks depend on the deformation induced in the rock mass. The in-situ porosity and permeability are low but change significantly with the disturbance and the associated strain. The permeability of coal is fracture-driven, and it decreases with the closure of rock fractures and vice versa (Figure 2.7). A typical stress-strain-permeability curve is defined in three zones: elastic, plastic softening, and residual state. In the elastic zone, the permeability decreases with an increase in the axial strain as the existing cracks and pore spaces close during this stage (Xiao et al., 2020; Zhou et al., 2020). The permeability increases significantly as new cracks and fractures develop in the rock in the plastic softening and residual stress stages (Zhang 2021b).

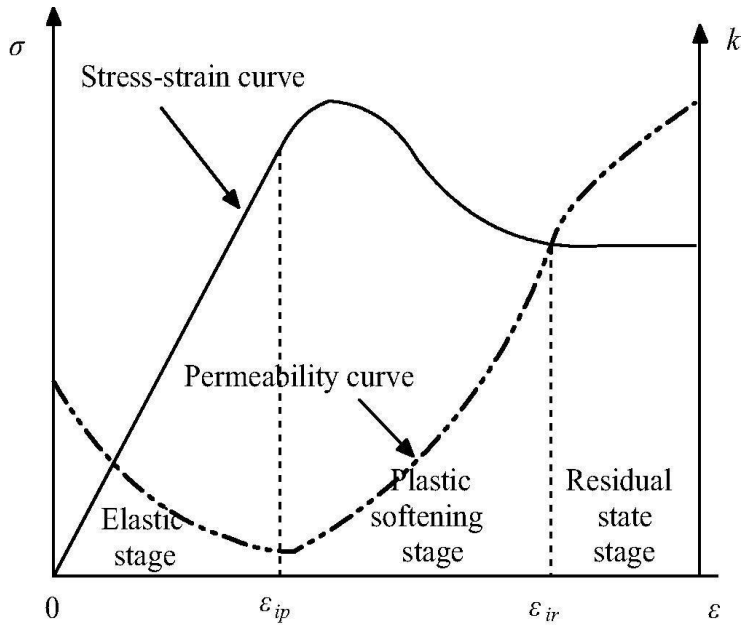

Figure 2.7. Stress-strain-permeability for coal samples (**Xue et al., 2017**)

In the last few decades, Dabbous et al. (1973), Durucan (1981), Harlow and LeCain (1993), Luo et al. (2001), Ren and Edwards (2002), Whittles et al. (2006), and Zhu et al. (2015) developed a series of relationships (Table 2.3) for the estimation of strain-dependent

permeability. Yang et al. (2007) developed a flow-stress-damage coupled model based on the damage mechanics to link the evolution of permeability with the accumulated damage. Meng et al. (2016) also confirmed that the permeability distribution in a structure varies with the constitutive behaviour. Primary pores close during elastic deformation but rapidly reopen after the peak strength. As the interstice dimensions in a coal seam are minimal, the fluid flow is laminar in such cases.

Table 2.3. Permeability relationships by various researchers

References	Permeability Relationship	Parameters
Zhu et al. (2015)	$k = k_o \left[\left\{\left(\frac{1}{n_o}\right)(1+e_v)^3\right\} - \left\{\left(\frac{1-n_o}{n_o}\right)(1+e_v)^{-1/3}\right\}\right]^3$ …(2.18)	n_0 is the initial porosity, ε_v is the volumetric strain; k_0 is the initial permeability
Durucan (1981), Whittles et al. (2006)	$K_f = K_{fo}\frac{(\sigma_1+\sigma_3)^{0.816}}{2}$ …(2.19)	K_f is the permeability of the fractured rock, m^2/pa.s; σ_1 and σ_3 are the maximum and minimum principal stresses, MPa; K_{fo} is the permeability, m^2/pa.s at $(\sigma_1+\sigma_3)/2$ =1 MPa
Ren and Edwards (2002)	$K_h = K_{ho}e^{-0.25*(\sigma_{yy}-\sigma_{yyo})}$ …(2.20) $K_v = K_{vo}e^{-0.25*(\sigma_{xx}-\sigma_{xxo})}$ …(2.21)	K_h and K_v are the horizontal and vertical permeability, m^2/pa.s; K_{ho} and K_{vo} are the initial permeability of the rocks in the horizontal and vertical directions, m^2/pa.s; σ_{yy} and σ_{xx} *are* stresses induced in vertical and horizontal directions, MPa; σ_{yyo} and σ_{xxo} are initial stresses in vertical and horizontal directions, MPa

Luo, Peng, and Zhang (2001)	$K = 8.7 \times 10^{-16}\left(e^{(-5.07\times10^{-3}\sigma_m)} + 5.85 \times 10^{-4}\sqrt[3]{0.007\sigma_m}\right)$ …(2.22)	K is the permeability, m^2/pa.sec; σ_m is the mean stress within the barrier, MPa
Harlow and LeCain (1993)	$K = 3.4 \times 10^{-18} e^{(-1.2\times10^{-5}\sigma_m)}$ …(2.23)	
Dabbous et al. (1973)	$K = 3.8 \times 10^{-19} e^{(-2.2\times10^{-5}\sigma_m)}$ …(2.24)	

In general, the permeability of the rock masses around the protective water barrier pillar is very low. In unfractured rock, the fluid flow is governed by the permeability of the matrix, which can be determined in the laboratory or the field by the Packer test in a borehole. Flow in fractured rocks, on the other hand, is governed by rock mass permeability as well as discontinuity characteristics. Discontinuities form the major flow channels in such structures. Field measurements for understanding flow characteristics are challenged by the frequency of discontinuities adjacent to the testing zone and the hydraulic gradient, which may lead to the opening of cracks due to excessive pressure (Priest, 1993). The permeability data expressed in terms of mobility coefficient for different rock types are given in Table 2.4.

Table 2.4. Categorization of rock permeability (**Priest, 1993**)

Mobility coefficient (m^2/pa.sec)	**Description**	**Examples**
$>10^{-10}$	High	Coarse sand and gravel
10^{-12} to 10^{-10}	Medium	Coarse sandstone, fine sand, and silts
10^{-14} to 10^{-12}	Low	Medium sandstone, limestone, silty clay
10^{-16} to 10^{-14}	Very low	Fine sandstone, limestone, clay
$<10^{-16}$	Impermeable	Igneous and metamorphic rock materials

The site-specific data of rock permeability for Indian coal measure rocks are not readily available, and the accompanying uncertainty of various measurement methods is also significant. Wide variations can be expected near joints, faults, paleochannels, slickensides, or laminations of contrasting lithology. Generally, the protective water barrier pillars are constructed in the discontinuity-free zone. The permeability of the rocks varies between 10^{-12} and 10^{-23} m^2 depending on pore pressure, hydraulic gradient, rock type, and depth (Neuzil, 1994). The permeability of rock for gas is 2-10 times higher than that of water (Faulkner, 2000; Tanikawa and Shimamoto, 2009). Table 2.5 compiles the permeability data expressed in terms of the mobility coefficient, as reported by various researchers.

Table 2.5 Mobility coefficient of coal

Sl. No.	Source	Mobility Coefficient (m^2/Pa.sec)	Measurement Methodology
1	Prusty (2015)	1.95×10^{-12}	laboratory testing
2	Wachel (2012)	4.89×10^{-9}	upper coal seam
		2.93×10^{-11}	fractured zone
3	Ghosh (2011)	$3.44 \times 10^{-13} - 1.18 \times 10^{-12}$	laboratory testing
4	Esterhuizen and Karacan (2005)	3.99×10^{-10}	coal face cleat
		9.97×10^{-11}	coal butt cleat
			carb. shale
5	Ramamurthy et al. (2003)	4.48×10^{-10}	coal seam
		1.49×10^{-10}	pictured cliffs
6	Kendorski and Bunnell (2007)	4.05×10^{-13}	empirical method
7	Luo et al. (2001)	7.59×10^{-11}	empirical method
8	Harlow and LeCain (1993)	6.53×10^{-13}	empirically established based on field test data
9	Xue (1989)	$2.8 \times 10^{-14} - 1.05 \times 10^{-11}$	laboratory testing
10	Miller and Thompson (1974)	4.03×10^{-13}	empirical method

11	Dabbous et al. (1973)	1.11×10^{-13}	empirical method
12	Kissell and Bielicki (1972)	$1.01 \times 10^{-11} - 1.01 \times 10^{-8}$	in-situ testing
13	Patching (1965)	$4.2 \times 10^{-13} - 7.7 \times 10^{-11}$	laboratory testing
14	Huang and Shelton (1962)	$1.01 \times 10^{-12} - 1.01 \times 10^{-7}$	laboratory testing
15	Tarasov (1960)	$9.9 \times 10^{-15} - 4.2 \times 10^{-11}$	laboratory testing

The behaviour of rock mass drastically changes in the presence of water as it penetrates the rock matrix under a pressure difference. Earlier, the pores were primarily occupied by air; subsequently, these pore spaces are occupied by water. It leads to an increase in moisture content, substantially reducing the rock's strength. The tensile strength, uniaxial compressive strength, modulus of elasticity, internal friction angle, and cohesion decrease in contact with water (Liu et al. 2010, Guo 2010). Wang et al. (2019) suggested a weakening coefficient-based approach to calculate the effect of moisture content on the cohesion, internal friction angle, elastic modulus, and uniaxial compressive strength (Figure 2.8). This estimated coefficient is a multiplier of their values in the dry condition.

The hydro-mechanical stability of the pillar becomes more critical and challenging with the increasing depth of working and the water head acting on the PWBP (Moebs and Sames, 1989). As the depth increases, the compressive stresses also increase, which leads to a reduction in pore spaces, causing a decrease in seepage rate (Singh, 1983). On the contrary, increased in-situ stresses produce more damaged zone facilitating considerable seepage rate across the barrier under high water heads (LaMoreaux et al., 2014; Shen et al., 2012; Liu et al., 2021).

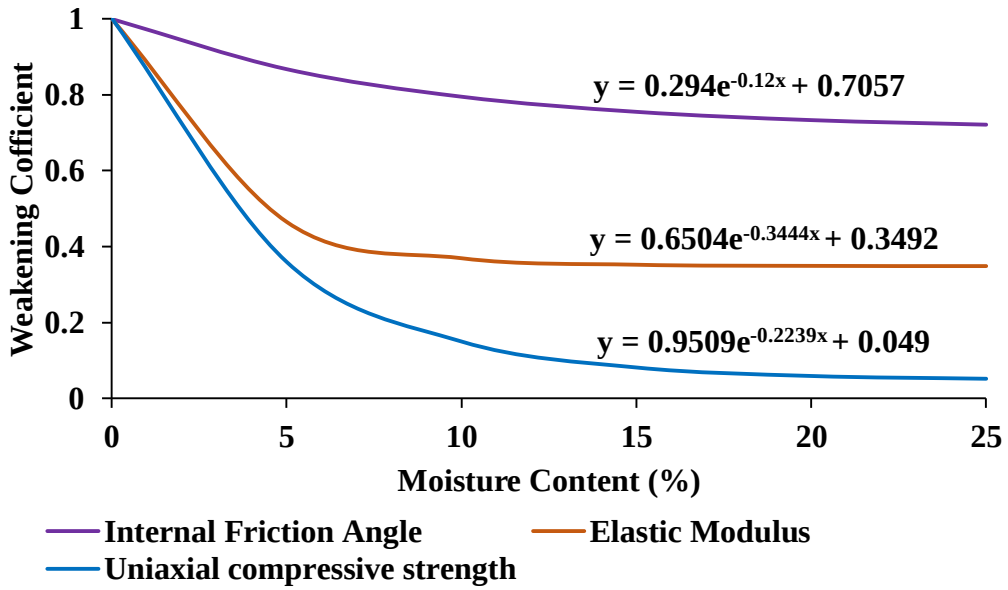

Figure 2.8. Weakening coefficient depending on moisture content (**Wang et al., 2019**)

The flow through discontinuities is strongly influenced by the depth of working. The cover depth governs the magnitude of normal stress at the interface and the plane of cracks or fractures across the structure. At shallow cover depth, the discontinuities are more conducive. With the increase in depth, the confining pressure increases along the discontinuities, which may lead to closure or reduced aperture of the discontinuities. However, the large induced load at higher depths increases the frequency of cracks and fractures in the pillars.

Discontinuities such as fractures, tension cracks, and faults are the primary sources to provide hydraulic interconnection, which is subjected to dilation and governs the flow characteristics (Rubio and Fabregas, 1998; Kendorski and Bunnell, 2007). Such discontinuities may break a portion of PWBP that creates a zone of very high permeability, thus reducing the effective width against the water reservoir (Zhu and Wei, 2011; Li and Wu, 2019; Mu et al., 2020).

Drainage management is critical for dealing with the excessive water seepage rate in the mine. If the pumping stops in the old abandoned waterlogged working, the water level rises,

and hence the hydraulic gradient and head acting along the PWBP also increase. This rise in water level increases hydraulic pressure, thereby increasing the water seepage rate. It necessitates proper analysis for the stoppage of pumping during the closure of deep mines.

It is not easy to estimate the seepage rate through PWBP in a mine. However, it can be estimated from the overall seepage rate maintained by the mine to assess the pumping efficiency. Natural groundwater that enters the underground workings by percolation through the intact overburden and seepage through broken strata is a significant contributor to mine water. The influx continues until the hydraulic balance between the water table in these areas and the surrounding areas is reached. The Government of India constituted the Groundwater Estimation Committee (GEC, 1997) to assess groundwater. Soni (2019) suggested that the GEC (1997) approach can be used to estimate the overburden seepage rate for an underground mine. Equation 2.25 shows the relation indicated by GEC for calculating the maximum feasible groundwater quantity Q_{mf} for a given lease area A_L, pit area A_p, the annual average rainfall R_a and rainfall infiltration factor R_{RIF}.

$$\mathrm{Q}_{mf} = \frac{A_L R_a R_{RIF}}{A_p} \qquad \ldots(2.25)$$

For consolidated sandstone, an infiltration factor of 0.05-0.07 is suggested.

2.8 Regulatory and Operational Provisions in Indian Coal Mines

As per regulatory provisions, a 60 m wide pillar is considered adequate for its safe performance in Indian coal mines. The DGMS circular (DGMS, 2003) stipulates that such pillars should be maintained between abandoned workings and contemporary mine developments in underground mines. An up-to-date 'joint survey plan' must also be

maintained as per clause (e) of sub-regulation 1, Regulation 65 of the CMR 2017. It should show all the features above and below ground up to 60 m from the boundary of the mine, including the working of neighbouring mines.

An up-to-date "water-danger plan" is required to be maintained as per Regulation 65 (1) (g(v)). It should outline all waterlogged workings in the vicinity of the underground mine that lies within 60 m of any part of the workings in any direction. As per sub-regulation 8 of Regulation 65, the Owner, Agent, and Manager should inform the neighbouring mine when they approach within 60 m of the settled or disputed boundary and also facilitate them to survey.

Regulation 150 of the CMR, incorporates the regulatory provisions for preventing the danger of inundation in underground mines. It suggests that proper arrangements should be made to prevent a sudden inrush of water in the mine, and no work should be done without the prior permission of the Chief Inspector as the working approaches within 60 m of any water accumulation zone. The work should be stopped immediately in case any abnormal seepage rate is observed. The height and width of the working should be restricted to a maximum of 2.4 m, and an exploratory borehole should be drilled to prevent accidental access into the waterlogged working. The height, width, and boreholes record should be maintained daily in a bound paged notebook made for this purpose, signed by a competent person, and countersigned by the Manager with the date every day. The plan and sections should be updated every 15 days under such conditions.

2.9 Summary

Inadvertent inundation has resulted in extensive losses in underground coal mines. One of the major causative factors leading to this hazard is the inadequacy of the width of the

protective barrier pillars. Among the various methods, as compiled in Table 2.1, the hydraulic performance-regulating parameters are hardly considered in any design approach. These methods are mainly experience-based and applicable to site-specific conditions only. Hence, a sincere effort at the laboratory and the field scale is required to narrow the prevailing understanding gap.

Protective water barrier pillars are engineering structures designed to provide mechanical stability and effective isolation against hydraulic pressure. The width-to-height (w/h) ratio defines the characteristic hydraulic profile for prevailing confining stress. A numerical model can be developed to evaluate the hydraulic performance of a barrier pillar and assess the water flow characteristics through the pillar system. It is essential to account for fluid flow through the barrier pillars to control stability. A field representative estimation of the permeability of the coal seam, the immediate floor, and the roof strata is also critically important. The literature review has manifested an absence of scientific know-how and poor standardisation for evaluating the performance of PWBP. The conventional approach for the design of such structures is limited to the assessment of mechanical strength, stress, and strain in the continuum medium.

While the general regulatory provisions mandate a minimum dimension of the pillar varying from 50 to 100 m in different countries without any consideration of the hydro-mechanical interaction, several empirical formulations have also been worked out to address this issue which estimates the size of pillar varying from 25-50 m at a cover depth of 100-350 m. The provisions of the Coal Mines Regulation in Indian geo-mining conditions mandate a 60 m wide protective water barrier pillar without considering mineral conservation, geo-mining,

or prevailing loading conditions. Such old-age conservative guidelines must be critically evaluated through scientific investigation to enable a rational design of protective pillars.

In most countries, modern legislation has changed, requiring the barrier pillars to be 'redesigned to accepted engineering standards'. Unfortunately, no such reliable method exists in Indian geo-mining conditions. It is always instructive to learn from the experience of other countries and make a suitable standard for Indian geo-mining conditions, aligning it with the accepted engineering standards. However, the methods developed elsewhere result in either over or underestimation of the pillar size as they only focus on the mechanical performance and ignore hydraulic performance. With increasing awareness regarding mineral conservation and the complexity of the pillar loading mechanism, it is essential to revisit the prevailing approach for ensuring the long-term stable performance of such pillars.

In the absence of well-established scientific know-how, the prevailing risk of mine inundation remains unknown for pillar width as small as 10 m on one side. On the other side, there is a significant loss of coal reserves for pillar width as large as 650 m. The issue is becoming critically important with the increasing depth of working. Hence, the need for a reliable assessment of the integrity of the existing barrier pillars and the rational dimension of new barriers under the increasing depth and age of the mine becomes most significant.